Biophysical Journal
Article

Biophysical Society

Using FCS to accurately measure protein concentration in the presence of noise and photobleaching

Lili Zhang,[1] Carmina Perez-Romero,[1,2,3] Nathalie Dostatni,[2,3] and Cécile Fradin[1,4,*]
[1]Department of Physics and Astronomy, McMaster University, Hamilton, Ontario, Canada; [2]Institut Curie, PSL University, CNRS, Paris, France; [3]Nuclear Dynamics, Sorbonne University, Paris, France; and [4]Department of Biochemistry and Biomedical Sciences, McMaster University, Hamilton, Ontario, Canada

ABSTRACT Quantitative cell biology requires precise and accurate concentration measurements, resolved both in space and time. Fluorescence correlation spectroscopy (FCS) has been held as a promising technique to perform such measurements because the fluorescence fluctuations it relies on are directly dependent on the absolute number of fluorophores in the detection volume. However, the most interesting applications are in cells, where autofluorescence and confinement result in strong background noise and important levels of photobleaching. Both noise and photobleaching introduce systematic bias in FCS concentration measurements and need to be corrected for. Here, we propose to make use of the photobleaching inevitably occurring in confined environments to perform series of FCS measurements at different fluorophore concentration, which we show allows a precise in situ measurement of both background noise and molecular brightness. Such a measurement can then be used as a calibration to transform confocal intensity images into concentration maps. The power of this approach is first illustrated with in vitro measurements using different dye solutions, then its applicability for in vivo measurements is demonstrated in *Drosophila* embryos for a model nuclear protein and for two morphogens, Bicoid and Capicua.

SIGNIFICANCE Many questions in cellular biology and biophysics would benefit from accurate measurements of protein concentration in vivo. For example, understanding how morphogen gradients are translated into target genes expression maps in developing embryos will necessitate determining absolute morphogen concentrations thatvary in space and time. Here, we propose a way to exploit fluorescence correlation spectroscopy data in samples prone to photobleaching to retrieve two crucial parameters, molecular brightness and background noise, which then allows one to turn confocal images into concentration maps. We demonstrate the efficacy of this method in fly embryos for three different nuclear proteins and suggest that it should be widely applicable to other types of eukaryotic systems.

INTRODUCTION

Many questions in cellular biophysics would benefit from accurate measurements of protein concentrations in live organisms (1,2), for example, understanding how morphogen concentration gradients are translated into expression domains of target genes necessitates determining morphogen concentration as it varies in space and time in developing embryos and tissues (3–10). In principle, fluorescence correlation spectroscopy (FCS), which allows measuring absolute concentrations of fluorescently tagged proteins noninvasively, should provide an ideal strategy to tackle this challenge. Single-point FCS is based on the quantification of the fluctuations in the fluorescence signal coming from a small confocal observation volume through the use of correlation functions (11,12). The signal is directly related to the Poisson-distributed number of observed mobile fluorophores, and knowledge of both its mean and standard deviation allows calculating absolute fluorophore concentration (13). This approach works very well in simple systems such as buffer solutions, but a number of issues arise when working with living systems.

Submitted April 5, 2021, and accepted for publication June 28, 2021.
*Correspondence: fradin@physics.mcmaster.ca
Editor: Stanislav Shvartsman.
https://doi.org/10.1016/j.bpj.2021.06.035

First, low biomolecule concentrations and high autofluorescence backgrounds often result in low signal/noise ratios in cells. This affects the ratio between the mean and the standard deviation of the signal and leads to a concentration overestimate. Correcting for this effect requires a precise measurement of the background fluorescence noise (14,15). Second, photobleaching of fluorescent proteins confined in the small volume of cells or cellular compartments causes a regular decrease of the protein population and fluorescent signal over time (16,17). This long-term photobleaching is an especially vexing issue because it not only leads to a concentration underestimate because of fluorophore depletion but also to the emergence of an additional timescale for the fluorescence fluctuations, which makes the interpretation of the FCS data more difficult. Photobleaching can be minimized by lowering excitation intensity; however, this comes at the cost of lowering the signal/noise ratio. Alternatively, the effect of long-term photobleaching in FCS data can be avoided by discarding or ignoring affected parts of the data (18–20) by considering only short time windows when correlating the signal (16,21–24) or by correcting the slow fluorescence decay with the help of an analytical function before correlating the signal (24,25). All of these methods, however, have drawbacks, and none of them allows analyzing uncorrected correlation functions, which is often the only type of data returned to the user by commercial FCS instruments.

Another important consideration is the heterogeneous and dynamic nature of living systems. Single-point FCS can give information about a few selected areas in the sample but cannot provide high throughput concentration data in space and time. FCS also fails to return proper concentrations if the environment is complex (e.g., because of the presence of membranes (26)) or if fluorophores form complexes or are immobile. One often-used workaround for these issues is to use single-point FCS to perform a calibration measurement in conditions in which the correct concentration can be recovered to obtain the molecular brightness B of a single fluorophore. Once B is known, confocal images acquired in the exact same conditions as the FCS measurement can be transformed into fluorophore concentration maps. This strategy has been used in a number of cases, for example, to measure the concentration of signaling proteins in *Escherichia coli* (27), histones in Hela cells (28), nuclear import factors at the nuclear pore complex (29), or morphogens in *Drosophila* embryos (5,18). A protocol detailing how to obtain FCS-calibrated concentration maps, including corrections for background and photobleaching, was recently published (30). A potential issue with this method, however, is that the molecular brightness of the fluorophore often has to be determined outside of the imaged area (e.g., buffer solution, cell with different expression levels, and different part of the cell or of the embryo) when it is known that B can vary a lot with environment (pH, buffer composition, and temperature (31,32)).

Building on these different ideas, we propose an original and direct way to obtain both fluorophore molecular brightness and background noise by using the artificial slow variation in fluorophore concentration due to photobleaching to build an in situ FCS calibration curve. These two quantities, in turn, make it possible to obtain very accurate FCS-calibrated concentration maps acquired just before performing the FCS calibration experiments. For this strategy to be successful, the issue of fitting correlation functions affected by slow photobleaching has to be tackled, which we explain how to do. We demonstrate the effectiveness of this strategy with a series of in vitro and in vivo experiments.

Theory

The autocorrelation function (ACF) of the fluorescence signal, $I(t)$, recorded during an FCS experiment is defined as follows:

$$G(\tau) = \langle I(t)I(t+\tau)\rangle \,/\, \langle I\rangle^2 - 1.$$

Simple form of the ACF

For a single fluorophore species with molecular brightness B and concentration $c(\vec{r},t)$, the recorded fluorescence signal is a function of the collection profile $W(\vec{r})$:

$$I(t) = \int BW\left(\vec{r}\right)c\left(\vec{r},t\right)d\vec{r}.$$

Both I and B are expressed in photons per second (or hertz). In a confocal instrument, $W(\vec{r})$ resembles a three-dimensional Gaussian ($1/e^2$ radius w, aspect ratio S), and the average detected signal is $I = \gamma BN$, where N is the average number of fluorophores in the effective detection volume $V = \pi^{3/2}Sw^3$, and $\gamma = 2^{-3/2}$ is a geometrical factor (33).

For a diffusive species (diffusion coefficient D) with a single dark state (exponential relaxation time τ_T, average fraction of dark molecules T), the ACF takes the following simple form (34):

$$G_D(\tau) = G(0)\frac{1 + T/(1-T)e^{-\tau/\tau_T}}{(1+\tau/\tau_D)\left(1+\tau/\left(S^2\tau_D\right)\right)^{1/2}}, \qquad (1)$$

where the characteristic diffusion time is $\tau_D = w^2/(4D)$ and the amplitude of the diffusive term is $G(0) = 1/N$.

If a second diffusive species is present, a second term needs to be added to this expression. As long as B is the same for both species (35), the following applies:where p

$$G_D(\tau) = G(0)\left(1+T\,/\,(1-T)e^{-\tau/\tau_T}\right)\left[\frac{p}{(1+\tau/\tau_{D1})\left(1+\tau/\left(S^2\tau_{D1}\right)\right)^{1/2}}+\frac{1-p}{(1+\tau/\tau_{D2})\left(1+\tau/\left(S^2\tau_{D2}\right)\right)^{1/2}}\right], \quad (2)$$

is the fraction of the first species and τ_{D1} and τ_{D2} are the diffusion coefficients of the first and second species, respectively. In this simple case (two species with same molecular brightness), the combined amplitude of both terms, $G(0)$, is related to the total number of fluorophores, N, as before: $G(0) = 1/N$.

Influence of background noise

In the presence of background noise with mean I_B, the average detected signal becomes the following:

$$I = \gamma BN + I_B = \gamma BN\left(1+\frac{m}{N}\right), \quad (3)$$

where we have defined the constant: $m = I_B/(\gamma B)$. The ratio N/m is a measure of the signal/noise.

As long as the background noise is uncorrelated, the ACF retains the same form as in the absence of noise (Eq. 1), but its amplitude decreases as N/m decreases (14,15):

$$G(0) = \frac{1}{N}\frac{1}{(1+I_B/[I-I_B])^2} = \frac{1}{N}\frac{1}{(1+m/N)^2}. \quad (4)$$

For a given amount of noise (that is a given value of m), $G(0)$ is maximum when $N = m$. If $N \gg m$ (high signal/noise ratio) we recover $G(0) \simeq 1/N$. However, in the limit where $N \ll m$, $G(0) \simeq N/m^2$ becomes proportional to N instead.

Equation 4 can be rewritten as a function of I, which in contrast to N is a quantity directly accessible through experiments:

$$G(0) = \gamma B\frac{I-I_B}{I^2}. \quad (5)$$

Influence of photobleaching

When fluorophores are confined to a small compartment, photobleaching may cause a slow decrease in the average number of fluorescent molecules. Consider the simple case of an exponential decrease of the fluorophore concentration:

$$\tilde{I}(t) = \gamma BN_0\left(e^{-\frac{t}{\tau_P}}+\frac{m}{N_0}\right), \quad (6)$$

where a tilde has been used to indicate averaging over a time much longer than the characteristic diffusion time, τ_D, yet much shorter than the characteristic photobleaching decay time, τ_P. N_0 is the average number of molecules in the detection volume at $t = 0$. The average signal between t_1 and t_2 is as follows:

$$\left\langle I\right\rangle_{t_1,t_2} = \gamma BN_0\left(\frac{\tau_P}{t_2-t_1}e^{-\frac{t_1}{\tau_P}}\left(1-e^{-\frac{t_2-t_1}{\tau_P}}\right)+\frac{m}{N_0}\right).$$

At any given time, the measured signal is the sum of $\tilde{I}(t)$ and of a fluctuation around this instantaneous average value due to fluorophore diffusion, $\delta I(t)$. Considering there is no correlation between these two contributions, we can write the following:

$$\langle I(t)I(t+\tau)\rangle = \left\langle \tilde{I}(t)\tilde{I}(t+\tau)\right\rangle + \langle \delta I(t)\delta I(t+\tau)\rangle. \quad (7)$$

The second term in Eq. 7 captures fluctuations in the number of fluorophores in the detection volume due to diffusion. As long as in-focus photobleaching is negligible, it gives rise to the same contribution as before in the ACF, given by Eq. 1. However, N now varies over the course of the measurement, and the amplitude of $G_D(\tau)$ is related to $\langle N\rangle$, the average value of N over the course of the measurement:

$$G(0) = \frac{1}{\langle N\rangle} = \frac{t_M/\tau_P}{N_0(1-e^{-t_M/\tau_P})}. \quad (8)$$

Importantly, because $\langle I\rangle = \gamma B\langle N\rangle$, the relationship between I and $G(0)$ (Eq. 5) is not modified by photobleaching.

The other term in Eq. 7 captures the slow decrease of the signal over time due to fluorophore photobleaching, resulting in a new term in the ACF, $G_P(\tau)$. Its exact expression depends on the normalization scheme used to calculate the denominator of the ACF (see Appendix). In the case of a symmetric normalization, the denominator is calculated using $\langle I\rangle_{0,t_M-\tau}\langle I\rangle_{\tau,t_M}$. This leads to the following expression for the photobleaching term of the ACF (in which the factor -1 present in the definition of the ACF has been included):

In the absence of background noise ($m = 0$), this expression reduces to that previously calculated by Bacia (36):

$$G_P(\tau) = \left(\frac{t_M - \tau}{2\tau_P}\coth\left[\frac{t_M - \tau}{2\tau_P}\right] - 1\right) \Bigg/ \left(1 + \frac{m}{N_0}\frac{t_M - \tau}{\tau_P}\frac{1 + e^{\tau/\tau_P}}{1 - e^{-\frac{t_M - \tau}{\tau_P}}} + \left(\frac{m}{N_0}\right)^2\left(\frac{t_M - \tau}{\tau_P}\right)^2\frac{e^{\tau/\tau_P}}{1 - e^{-\frac{t_M - \tau}{\tau_P}}}\right). \quad (9)$$

$$G_P(\tau) = \frac{t_M - \tau}{2\tau_P}\coth\left[\frac{t_M - \tau}{2\tau_P}\right] - 1. \quad (10)$$

The ACF is given by $G(\tau) = G_D(\tau) + G_P(\tau)$.

From pixel intensity to concentration

The relationship between the fluorescence intensity i (in photons per pixel) measured in a confocal image and the fluorophore molar concentration c can be established considering that, by definition, $N = \mathcal{N}cV$ (where $\mathcal{N}$ is Avogadro's number) and that i is related to N through Eq. 3: $i/\delta = \gamma BN + I_B$ (where δ is the pixel dwell time). In the end, the result is as follows:

$$c(x, y) = \frac{i(x, y)/\delta - I_B}{\mathcal{N}\gamma BV}. \quad (11)$$

MATERIALS AND METHODS

Fluorophore solutions

Alexa Fluor 488 (AF488) was purchased from Invitrogen (now Life Technologies, Carlsbad, CA). It has a known diffusion coefficient $D = 435\ \mu m^2/s$ at 22.5°C (37). Solutions of AF488 were prepared in double-deionized water (resistance 18 MΩ). Purified enhanced green fluorescent protein (eGFP) was purchased from BioVision (catalog number: 4999; Milpitas, CA). This protein is labeled with two polyhistidine tags, and its molecular weight (32.7 kDa) is slightly larger than that of wild-type GFP. Solutions of eGFP were prepared in phosphate buffer saline.

Drosophila embryos

Drosophila embryos were prepared for imaging following the protocol described in (38). *Drosophila melanogaster* fly strains expressing nuclear localization signal (NLS)-eGFP, Bicoid (Bcd)-eGFP (a kind gift of Dr. Wieschaus) (5), or Capicua (Cic)-sfGPP (a kind gift of Dr. Shvartsman) (39) were stored and maintained in a 25°C incubator with alternating day-night lighting. To collect embryos for experiments, plastic tubes containing flies were inverted on an embryo collection plate with yeast paste in the center. After ~3 h, the embryos on the collection plate were transferred with a tweezer to a double-sided tape to remove the chorion. The dechorionated embryos were then transferred onto a thin layer of heptane glue on a 0.17-mm coverslip. The ventral side of the embryo was placed in contact with the glue such that as many nuclei as possible could be observed just above the coverslip. Lastly, a small drop of Halocarbon oil 700 (Sigma-Aldrich, St. Louis, MO) was added on top of the embryos to prevent evaporation while allowing oxygen permeation into the embryo.

FCS and confocal imaging

Single-point FCS data and confocal images were both recorded on an Insight Cell confocal microscope (Evotec Technologies, now PerkinElmer, Waltham, MA) using the same configuration. Fluorescence was excited with a 488-nm continuous wave solid state diode-pumped laser (Sapphire 488–20/460-10; Coherent, Santa Clara, CA). The excitation power was 75 μW when working with AF488 and 25 μW when working with eGFP in vitro. It was 20 μW when working with embryos expressing NLS-eGFP or Bcd-eGFP, and 25 μW when working with embryos expressing Cic-sfGFP. The excitation beam was set so as to underfill the back aperture of the water-immersion objective (UAPON, ×40, 1.15 NA; Olympus, Tokyo, Japan) and was used in conjunction with a 40-μm pinhole in the detection pathway. All experiments were performed at room temperature. Single-point FCS measurements of 5, 10, or 20 s were performed for 10, 20, or 40 repeats in each series. Fitting of the ACF obtained as a result of single-point FCS experiments was done either with the software FCS+plus Analyze (Evotec Technologies, now PerkinElmer, Waltham, MA) or with MATLAB (The MathWorks, Natick, MA).

RESULTS

We carried a series of FCS experiments, both in vitro and in vivo, to confirm the relationship between $G(0)$, the amplitude of the diffusive part of the ACF, and I, the mean count rate, which are both experimentally accessible quantities. This relationship is predicted to obey Eq. 5 and should depend on the values of the fluorophore molecular brightness (B) and the noncorrelated average background noise (I_B). Varying $G(0)$ and I, which can be achieved by systematically varying the fluorophore concentration, should allow one to retrieve the two crucial calibration parameters, B and I_B, and to calculate absolute fluorophore concentration directly from I.

In vitro: AF488 and eGFP

Single-point FCS experiments were performed on two types of in vitro samples: AF488 and eGFP solutions, in which fluorophore concentration was varied over several orders of magnitude by performing serial dilutions. Both samples serve as a model system for fluorophores undergoing free diffusion in the absence of photobleaching, giving the opportunity to explore the relationship between $G(0)$ and I in a simple system. Results from these experiments are shown in Fig. 1.

The ACFs obtained as a result of these experiments are, as expected, well fitted with a one-component model (Eq. 1),

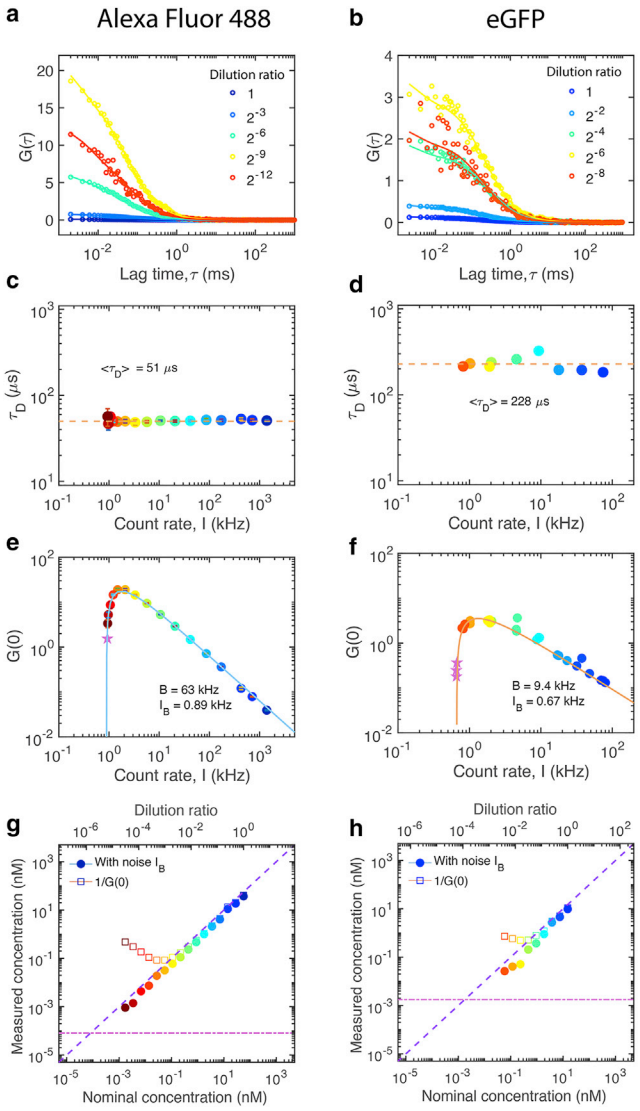

FIGURE 1 Single-point FCS concentration measurements in solution: AF488 (*left column*) and eGFP (*right column*). (*a* and *b*) Example of ACFs obtained at different concentrations (while the excitation power was kept constant). Solid lines are fitted with Eq. 1. (*c* and *d*) Characteristic relaxation time, τ_D, extracted from the ACFs and plotted as a function of count rate, I. Dashed line shows the mean τ_D. (*e* and *f*) Relationship between $G(0)$, the amplitude of the diffusive part of the ACF, and I, the mean count rate. The solid line is a fit with Eq. 5, which allows the extraction of both molecular brightness, B, and background noise, I_B. Pink stars represent data from the buffers for which very small amounts of contaminant gave rise to a detectable ACF. In (*f*), data points of the same color show the result from repeated measurements in the same sample. (*g* and *h*) Absolute concentration calculated from the estimated value of N. Open symbols show what happens when background noise is ignored (i.e., when assuming that $N = 1/G(0)$), whereas solid symbols show what happens when noise is taken into account (i.e., when using Eq. 4 to solve for N given the value of $m = I_B/(\gamma B)$ obtained from the fit of the dependency of $G(0)$ on I shown in *e* and *f*). The purple dashed line shows the nominal fluorophore concentration (provided by the suppliers), and the pink dotted dashed line shows the estimated value of the contaminant concentration in the buffer. To see this figure in color, go online.

assuming the presence of a single population of fluorophore in solution (Fig. 1, *a and b*). The characteristic diffusion times extracted from these fits are constant throughout the explored concentration range (Fig. 1, *c and d*). Their mean values ($\langle\tau_D\rangle = 51 \pm 3$ μs for AF488 and 228 ± 43 μs for eGFP, corresponding to diffusion coefficients of 435 and 97 $\mu m^2/s$, respectively) are in keeping with the respective molecular weight of the two fluorophores (0.72 kDa for AF488 and 32.7 kDa for eGFP). In sharp contrast to τ_D, the amplitude of the diffusive part of the ACF, $G(0)$, varied over two to three orders of magnitude as the fluorophore concentration was varied (Fig. 1, *e and f*).

It is often assumed when using FCS data to measure concentration that $G(0)$ is simply inversely related to the average number of fluorophores present in the confocal detection volume ($G(0) = 1/N$). In that case, we should see a monotonous increase of $G(0)$ as the fluorophore is diluted and as the count rate decreases, as is indeed observed at high fluorophore concentrations (high count rate). However, as I approaches the count rate measured for the buffer, $G(0)$ reaches a maximum and then sharply decreases (Fig. 1, *e and f*). This is what is expected in the presence of uncorrelated background noise, an effect that is captured in Eq. 5. Fitting of the data shows an excellent agreement with Eq. 5 and allows retrieving of two very important parameters—the fluorophore molecular brightness B and the background noise I_B. From these parameters, the ratio $m = I_B/(\gamma B)$ can be calculated, which gives an idea of how large background noise is compared with the effective brightness of a single molecule. We found that $m = 0.014$ for AF488 and 0.071 for eGFP, reflecting a large difference in molecular brightness for these two fluorophores.

Once the value of m is known for a particular sample and a particular set of experimental conditions, the actual relationship between $G(0)$ and N (Eq. 4) can be used to calculate N from the measured value of $G(0)$. The absolute fluorophore concentration can then be calculated using the value of V (observation volume) obtained from ACF measurements with a fluorophore with known diffusion coefficient (AF488). The concentrations measured for the AF488 and eGFP samples as a function of their dilution ratio are shown in Fig. 1, *g and h*. Strikingly, a linear relationship between these two quantities is obtained over the whole measurement range for both samples, showing that FCS allows precise concentration measurements in the sub-nanomolar range. Comparing these results (*solid symbols* in Fig. 1, *g and h*) with those obtained without taking into account background noise (*open symbols*) shows that the procedure described here extends the accessible concentration range by approximately two orders of magnitude. We note that for both fluorophores, the concentrations measured by FCS were about 30% smaller than the nominal concentrations indicated by the suppliers (*dashed lines* in Fig. 1, *g and h*), which is not overly surprising because fluorophores might improperly dissolve or adsorb on sample surfaces or photobleach.

Although the precision of the concentration measurements and their accessible range (down to 1 pM for AF488 and 20 pM for eGFP) are impressive for both fluorophores, it is noticeably lower for eGFP. This difference may be attributed in part to a certain instability of the eGFP sample (visible in the dispersion in the values of $G(0)$ measured for repeated measurements; Fig. 1 *f*) probably because of the presence of aggregates and to the interaction of the protein with the surfaces of the sample chamber. Mostly, it can be traced back to the relatively lower molecular brightness of eGFP and consequently larger m. We found that the lowest attainable concentration was about two orders of magnitude lower than that for which $G(0)$ reaches a maximum. Because the peak in the value of $G(0)$ is attained when $N = m$, the lower the value of m, the lower the concentration that can be directly measured by single-point FCS.

In vivo: NLS-eGFP, Bcd-eGFP, and Cic-sfGFP

In cells, systematic variations in apparent fluorophore concentration can be achieved through gradual photobleaching of the molecules present inside the cellular compartment where single-point FCS measurements are performed. We used this effect to establish the relationship between $G(0)$ and I inside the nuclei of live embryos. We used *D. melanogaster* embryos expressing different types of fluorescent protein fusion for which we can expect different dynamics, molecular brightness, and concentration: an NLS-eGFP, a transcription activator called Bcd-eGFP, and a transcription repressor called Cic-sfGFP. Both Bcd and Cic are important regulators of gene expression that are endogenously expressed during early fly development.

We performed series of 10–20 single-point FCS measurements (for durations of 5–20 s) at the center of nuclei in the midsection of embryos during nuclear cycle 13 or 14, as illustrated in Fig. 2 for NLS-eGFP. All three studied proteins are actively imported and accumulate into nuclei, resulting in the presence of brightly fluorescent nuclei in images of the cortical region of the embryo, where a single layer of nuclei is found at this stage of development (Fig. 2 *a*). The depletion of fluorescence due to continuous photobleaching during repeated FCS measurements in a single

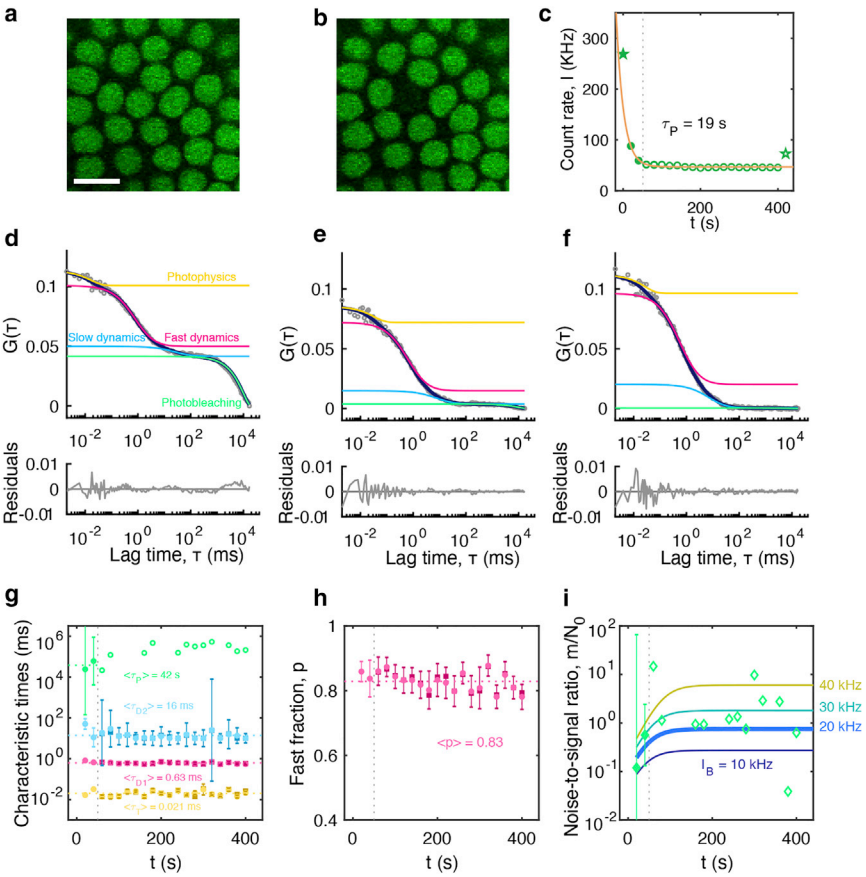

FIGURE 2 Single-point FCS measurements in *D. melanogaster* embryos expressing NLS-eGFP. (*a*) Representative confocal image of a field of nuclei in the cortical region of the embryo. Scale bar, 10 μm. (*b*) Same field of view, just after a series of 20 single-point FCS measurements. The nucleus where the FCS measurements were performed is only very faintly fluorescent. (*c*) Average count rate recorded for each of the 20 FCS measurements (*solid* and *open circles*, separated by *vertical dashed lines*, indicate measurements during which the count rate either significantly varied or was reasonably stable). The orange line is an exponential fit to the data (Eq. 6). The count rate recorded for the pixel at which the FCS measurements were performed is also shown for the image acquired just before ($t = 0$ s) and just after ($t = 420$ s) the FCS measurements (*star symbols*). (*d–f*) ACF obtained for the first (*d*), second (*e*), and 20th (*f*) measurements in this series of 20-s FCS measurements. Solid lines indicate a fit with a two-component model, taking account the possibility of photobleaching (Eqs. 2 and 9), and residuals are shown below. Lines of different colors indicate the different decays observed in the ACF due to triplet state relaxation (*orange*), fast diffusion (*magenta*), slow diffusion (*blue*), and photobleaching (*green*). (*g*) Different characteristic times, (*h*) fraction of fast molecules, and (*i*) noise/signal ratio obtained from the fit of the ACF for all the measurements in the series. Error bars in (*g*)–(*i*) correspond to 50% confidence intervals, except for m/N_0, for which the error bars correspond to 10% confidence intervals (values obtained from ACFs with a photobleaching decay too small for a reliable estimate are indicated by *open symbols*, and without error bars because they were out-of-range; a few fits did not converge properly for these parameters, in which case they were not shown). In (*g*) and (*h*), circles and squares correspond to values obtained from fits performed with and without the photobleaching term, respectively. Horizontal dashed lines indicate average values (for τ_P only reliable measurements, indicated by *solid symbols*, have been considered when calculating this average value). In (*i*), the solid lines indicate the predicted value of $m/N_0 = I_B/(I - I_B)$ for different values of I_B, approximating I by its fitted value (*orange line* in *c*). To see this figure in color, go online.

nucleus was evident in images taken immediately after these measurements, in which the fluorescence of the studied nucleus strongly diminished (Fig. 2 *b*). The decay in the fluorescence signal at the position of the FCS measurements, which can be attributed to the photobleaching of the nuclear fraction of NLS-eGFP, was well approximated by a single exponential. In a regular cell, the cytoplasmic fraction of the fluorescent protein would also eventually get photobleached over a time corresponding to nucleocytoplasmic exchange—resulting in an additional slower decay time. But because the fly embryo is a syncytium, the cytoplasmic concentration remains constant over experimental timescales, and only a single exponential decay is observed. The characteristic time associated with this decay is $\tau_P \approx$ 20 s in the conditions of our experiments (Fig. 2 *c*). Thus, after only a few measurements, an equilibrium is reached between the import of new fluorescent molecules into the nucleus and the photobleaching, allowing the fluorescence to stabilize. When excitation is stopped at the end of the series of measurements, the fluorescence immediately starts recovering because of nuclear import (*green star* in Fig. 2 *c*).

The strong photobleaching that occurred during the first few FCS measurements in a series resulted in a visible decay in the ACF around τ_P, i.e., at much larger lag times than the decay corresponding to the motion of the proteins (Fig. 2, *d and e*). In contrast, the ACFs corresponding to later measurements in the series, after stabilization of the fluorescence, did not show this large time decay (Fig. 2 *f*). We therefore fitted our data with a model that included a two-component diffusive term (Eq. 2, because most nuclear proteins show at least two mobile components (28,35,40,41)) and a term corresponding to long-term photobleaching (Eq. 9; see Theory for a derivation of this term). This model allowed adequately fitting of all measurements in a series (for all studied proteins), as shown for NLS-eGFP in (Fig. 2, *d–f*), and retrieving four different characteristic times (for photophysics, fast diffusion, slow diffusion, and photobleaching; Fig. 2 *g*) for each of them; the fraction of fast molecules p obtained from the relative amplitude of the fast and slow diffusion terms (Fig. 2 *h*); and an estimate of the noise/signal ratio m/N_0 obtained from the amplitude of the photobleaching term (Fig. 2 *i*). This last parameter is reliably obtained only for the first few measurements in a series (*solid symbols* in Fig. 2 *i*), when the photobleaching decay is clearly visible in the ACF (later measurements can be fitted without the photobleaching term). Over these first few measurements, the relative importance of noise increases by several orders of magnitude. In this case, it appears to stabilize around a value of $m/N_0 = 1$, indicating that about half of the detected signal at this point comes from background fluorescence. This is consistent with the contrast observed in Fig. 2 *b*, where the studied nucleus is visible, but just barely.

For concentration measurements, however, the most important information contained in the ACFs is the amplitude of the combined diffusion terms, $G(0)$. For each series of FCS measurements that was performed (between 5 and 7 for each protein, performed in different embryos and on different days but using the same experimental conditions), the values obtained for $G(0)$ were found to depend on the count rate I as expected and as captured in Eq. 5 (Fig. 3, *a, d, and g*). For each series of successive measurements, fit of the data with Eq. 5 allowed a reliable in situ measurement of both molecular brightness B (Fig. 3, *b, e, and h*) and background I_B (Fig. 3, *c, f, and i*), just as for the fluorophore solutions described in the previous section. As long as the count rate was corrected for uneven illumination and detection across the field of view (as explained in the next section), the values of I_B were found to be similar for embryos expressing different proteins, ~10–15 kHz in the conditions of our experiments. The values of B were also reproducible but varied for different proteins and decreased from NLS-eGFP to Bcd-eGFP to Cic-sfGFP. As expected, the importance of noise was much larger in embryos than in solution, as demonstrated by the average values of m that were observed: $m = 2.5$ for NLS-eGFP, 4.3 for Bcd-eGFP, and 7.2 for Cic-sfGFP, indicating that measuring very low concentrations will be much more challenging in this case. Interestingly, for NLS-eGFP and Bcd-eGFP, the equilibrium concentration reached after several FCS measurements was still well above the point at which $G(0)$ starts noticeably decreasing because of background noise (Fig. 3, *a and d*), whereas for Cic-sfGFP, a strong decrease in $G(0)$ is observed for the later measurements in each series, and very low concentrations (for which $N < m$) are achieved at that point (Fig. 3 *g*). This difference can be traced back to the different behavior of these proteins in regard to nuclear import. -Whereas the nuclear concentration of fluorescent Bcd-eGFP and NLS-eGFP can completely recover in only a few minutes if a whole nucleus is photobleached (5), Cic-sfGFP only incompletely recovers (42), suggesting that the available pool of Cic in the cytoplasm of the embryo is very limited. Thus, the nuclear concentration reached at long times as an equilibrium between photobleaching and nuclear import is much lower for Cic than it is for the other two proteins. As a result, the estimate of B that can be made from each individual ACF by neglecting the effect of noise (i.e., using $B = G(0)I/\gamma$) only differs from the actual B by at most ~30% for NLS-eGFP and ~50% for Bcd-eGFP (Fig. 3, *b and e*, *small symbols*). But for Cic-sfGFP, the error made on the value of B when neglecting background noise can approach ~100% (Fig. 3 *h*).

Obtaining concentration maps

To obtain concentration maps of fluorescent proteins from confocal images, we followed the procedure illustrated in Fig. 4 for a *D. melanogaster* embryo expressing Cic-sfGFP.

First, a confocal image was acquired in the cortical region of the midsection of the embryo, just above the coverslip to

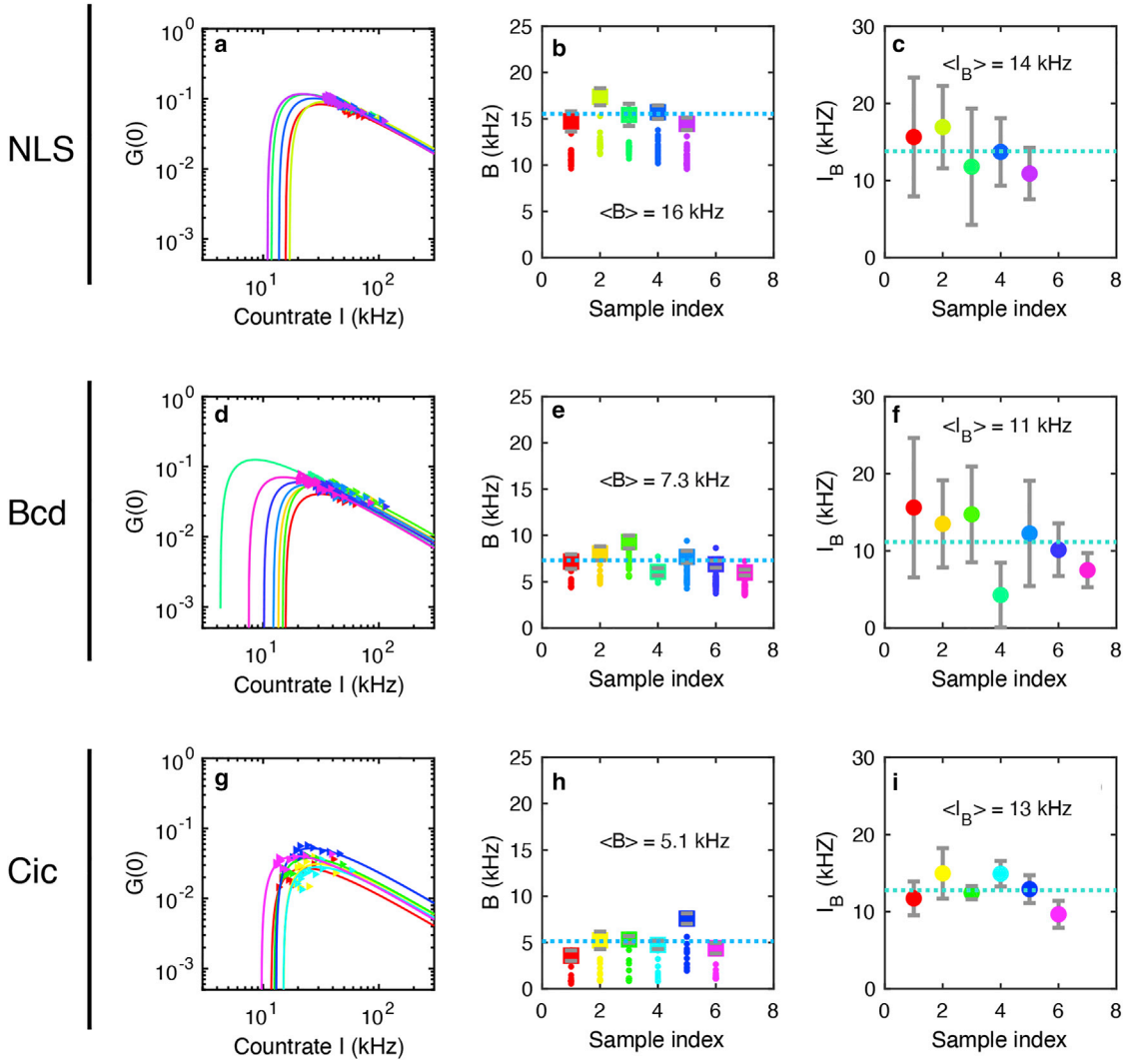

FIGURE 3 Relationship between $G(0)$, the amplitude of the diffusive part of the ACF, and I, the calibrated mean count rate, for embryos expressing NLS-eGFP (*a–c*, *top row*), Bcd-eGFP (*d–f*, *middle row*), and Cic-sfGFP (*g–i*, *bottom row*). (*a*, *d*, and *g*) For each type of embryo, at least five series of FCS measurements were performed, each resulting in a $G(0)$ vs. I sequence (represented by *symbols* of the *same color*), which was fitted with Eq. 5 (*lines*). (*b*, *e*, and *h*) Molecular brightness B (*large symbols*) and (*c*, *f*, and *i*) background noise I_B extracted from the fits of each of the $G(0)$ vs. I sequence. Error bars correspond to the 95% confidence interval obtained for these parameters. The mean values of B and I_B are indicated by a dashed line. In (*b*), (*e*), and (*h*), the values of B recovered from each individual FCS measurement, assuming $G(0) = \gamma B/I$ (no noise) is also shown (*small symbols*). To see this figure in color, go online.

reduce optical aberrations (Fig. 4 *a*). The original image was then corrected for the spatially uneven illumination and detection efficiency of our confocal instrument (Fig. 4 *b*). A previously acquired image of an AF488 solution for the exact same field of view was fitted to a broad two-dimensional Gaussian function, which was then normalized to 1, after which the pixel intensity at each point of the image was divided by the value of this normalized Gaussian function. The corrected intensity map then correctly displays nuclei with uniform fluorescence intensity across the field of view (Fig. 4 *b*), as expected here because Cic is known to have a uniform nuclear concentration in this region of the embryo (42).

The values of B and I_B measured in situ by performing a series of single-point FCS experiments (as explained in the previous section) were then used to convert the corrected intensity map into an absolute concentration map using Eq. 11 (Fig. 4 *c*). The single-point FCS measurements can be performed right after the acquisition of the image itself in the exact same field of view, or if the values of B and I_B can be shown to be reproducible for different regions of the sample, before imaging but in a different field of view (it is important that no FCS experiment is performed in the field of view before imaging to avoid photobleaching). It is also important that the intensity I used when fitting the dependence of $G(0)$ on I to obtain B and I_B is corrected for uneven illumination and detection in the same way as the pixels in the corrected image. A cross section through the concentration map shows that at this stage of development the nuclear concentration of Cic-sfGFP is ~200 nM (Fig. 4 *d*).

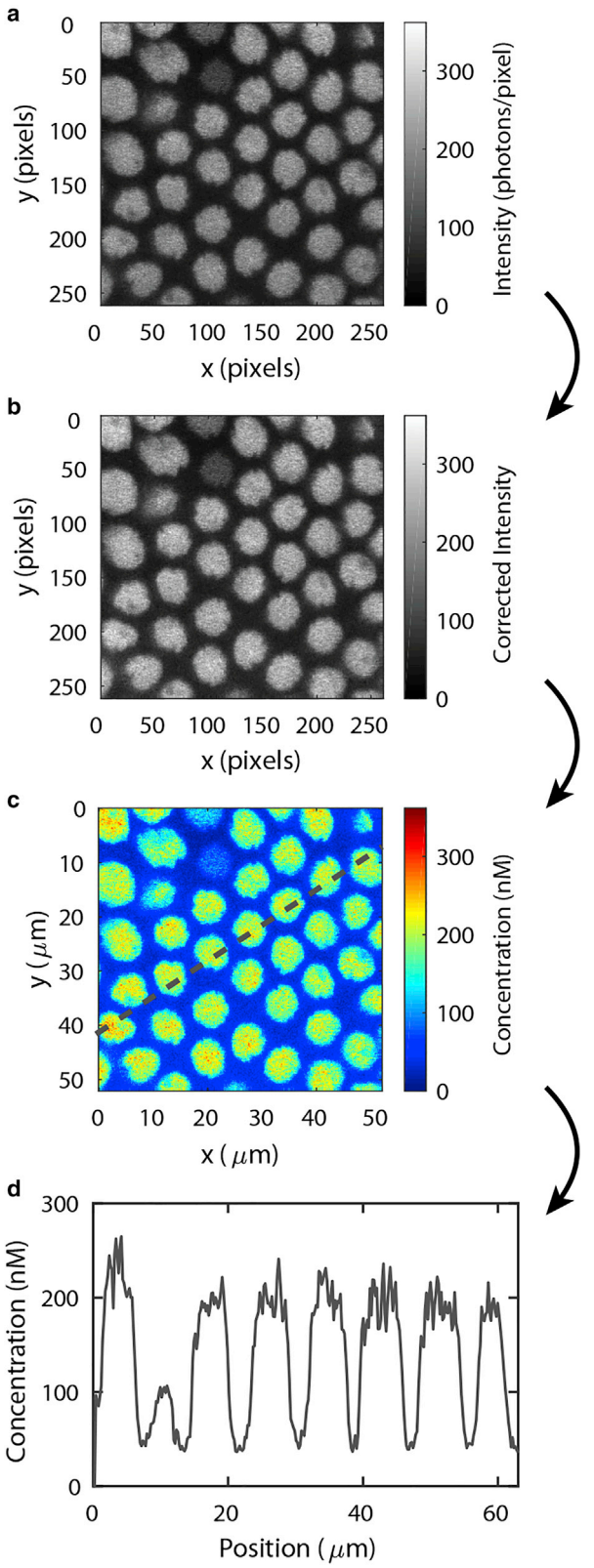

FIGURE 4 Conversion of an intensity image into a concentration map. (*a*) Confocal image of the cortical area in the midsection of a *D. melanogaster* embryo expressing Cic-sfGFP at nuclear cycle 14, ~1 h into the embryo development (261 × 261 pixels, pixel dwell time δ = 1 ms, pixel size 0.2 μm/pixel). (*b*) Intensity map after a correction taking into in account the uneven illumination and detection efficiency across the field of view. (*c*) Absolute concentration map calculated from the corrected pixel intensity map shown in (*b*), using Eq. 11 and values of B, I_B, and V obtained from single-point FCS data. (*d*) Concentration profile along the dashed line shown in (*c*). To see this figure in color, go online.

DISCUSSION

We propose here a method to obtain protein concentration maps that combines the strengths of confocal imaging (fluorescence signal measured in space and time and sensitivity to both immobile and mobile fluorophores) to those of FCS (sensitivity to absolute particle number) and, therefore, allows rapid measurements of absolute fluorophore concentration over large fields of view and with good temporal resolution. Obtaining a concentration map from a confocal image requires knowledge of both the molecular brightness B of the fluorophores present in the sample and the background intensity I_B. Our method is based on an accurate measurement of B that takes into account the effect of noise to avoid any systematic bias and that is performed in situ to recover the actual value of B in the cellular environment. We have demonstrated here through a series of in vitro and in vivo experiments that this could be achieved by establishing the dependence of $G(0)$ (a parameter directly accessible from FCS measurements) on I (average count rate), which we showed can be done by taking advantage of photobleaching, which causes a progressive decrease of I and provides the mean of performing a systematic titration of fluorophore concentration, just as one would do in vitro through serial dilutions. This strategy will be especially useful in systems in which photobleaching is prominent anyway or in which variations in concentration cannot be achieved by any other mean (e.g., uneven concentration across the sample or varying expression levels from cell to cell). Our approach should therefore be widely applicable to many types of eukaryotic systems.

It is important to note that some limitations are of course associated with the method proposed here. First, although the dependence between $G(0)$ and I captured in Eq. 5 is largely independent of the nature of the protein motions (it still holds for example if protein fractions with different mobilities are present), it relies on the assumption that the protein of interest has a mobile fraction with a single molecular brightness. Thus, Eq. 5 cannot be used in cases when the studied protein forms diffusing homo-oligomers. The method described here also relies on the assumption that the protein of interest is the only diffusing fluorescent species in the sample because the only type of noise considered in this work was uncorrelated noise (i.e., noise with no associated characteristic correlation time or with a correlation time outside of the 1-μs-to-10-s measurement window). Most types of noise expected in FCS experiments (detector noise, Rayleigh and/or Raman scattering, reflections at interfaces, and out-of-focus signal coming from fluorescent molecules) fulfill this condition. However, diffusing contaminants present in the detection

volume and with a concentration and molecular brightness comparable with that of the protein of interest would appear as an additional diffusion term in the ACF, changing its amplitude and throwing off concentration estimates. Contaminants present at very small concentrations (such as the sub-picomolar concentration of contaminant detected in buffer solutions in the presented in vitro experiments; indicated with a *dashed line* in Fig. 1, *g and h*) do not interfere with concentration estimates.

Second, only the long-term effect of the photobleaching occurring throughout the light cone and resulting in a slow exponential depletion of the fluorophore was considered here. The short-term effect of in-focus photobleaching on the ACF (as described, for example, in (43–45)) was not taken into account, although we expect that in most cases it would have a negligible effect on the retrieved value of $G(0)$—and therefore on the precision of concentration measurements. Third, even if $G(0)$ is correctly measured, the value of I_B can be obtained with good precision only if the regime in which $N < m$ (left of the inflection point on the $G(0)$ vs. I curve, when noise dominates) is reached. If only the regime in which $N > m$ is explored (as was the case here for NLS-eGFP or Bcd-eGFP that are continuously and robustly imported from the embryo's large cytoplasm and for which the $N < m$ regime was not reached; see Fig. 3, *a and d*), then B is precisely measured (Fig. 3, *b and e*) but not I_B (Fig. 3, *c and f*). Luckily, when it comes to concentration measurements, for these samples in which the signal/noise is always high (where $N \gg m$ and therefore $I - I_B \gg I_B$), uncertainties on I_B only result in small relative uncertainties on the measured absolute concentrations. For samples in which both the $N > m$ and $N < m$ regimes are spanned, as was the case here for Cic-sfGFP (for which nuclear import is limited, and the inflection point was reached on the $G(0)$ vs. I curve; see Fig. 3 *g*), a precise measurement of both molecular brightness and noise can be achieved (Fig. 3, *h and i*). In cultured cells, with a small cytoplasmic volume, nuclear import should always be limited by the finite available pool of cytoplasmic fluorescent proteins, and we therefore expect to always be in this favorable case. The method demonstrated here in fly embryos will thus be readily applicable in cultured cells, with the caveat that a double-exponential decay of the intensity might be expected.

Finally, a lot of possible artifacts (optical aberrations and fluorescence saturation) may affect the real or perceived size and shape of the confocal detection volume (46–49) and thus lead to systematic errors when using the value of the confocal volume V to calculate absolute protein concentrations from the estimated N (Eq. 11).

CONCLUSIONS

One tenet of our method is a systematic consideration of the effect of noise: when calculating absolute concentrations from pixel intensity (Eq. 11), when estimating B from $G(0)$ (Eq. 5), and when fitting the slow decay in the ACF due to photobleaching (Eq. 9). This proper accounting of noise means that we are able to accurately measure concentrations in cells, as intended. When applied to single-point FCS experiments, this relatively simple noise correction also means that we are able to measure picomolar concentrations in ideal fluorophore solutions (Fig. 1), lower than what is usually considered the lower limit for FCS measurements and entering instead the realm of what can be achieved using single particle detection (50,51).

Another tenet of our method is the fitting of ACFs that display a long-term decay due to photobleaching, for which we have developed a model (captured in Eq. 9) that incorporates both the effects of long-term photobleaching and background noise. This allows us to obtain accurate values for $G(0)$ because the count rate is continuously decreasing because of photobleaching, allowing us to explore the dependence of $G(0)$ on I over a wider range of count rates and to obtain as accurate an estimate of B as possible. Importantly, being able to fit ACFs that display photobleaching decays means that information about the dynamics of the fluorophores can be obtained from high signal/noise ratio data acquired at high excitation intensity and for long (10 s or more) measurement times and without having to wait until after the signal has stabilized to a low value. It resolves the conundrum of having to use low excitation intensities to avoid photobleaching at the cost of achieving only poor molecular brightness. We therefore expect it will change the way we think about performing single-point FCS experiments in cells by removing the obligation to avoid photobleaching at all costs.

APPENDIX: PHOTOBLEACHING TERM FOR DIFFERENT TYPES OF NORMALIZATION

The numerator of the ACF can be calculated as $\langle I\rangle^2_{0,t_M}$ (very simple normalization), $\langle I\rangle^2_{0,t_M-\tau}$ (simple normalization), or $\langle I\rangle_{0,t_M-\tau}\langle I\rangle_{\tau,t_M}$ (symmetric normalization).

In the first case (very simple normalization), we obtain the following:

$$G_P(\tau) = e^{-t_M/\tau_P}\frac{\frac{\sinh[(t_M-\tau)/\tau_P]}{(t_M-\tau)/\tau_P}}{\left(\frac{1-e^{-t_M/\tau_P}}{t_M/\tau_P}\right)^2} - 1. \tag{12}$$

In the second case (simple normalization), we obtain the following (36):

$$G_P(\tau) = \frac{t_M-\tau}{2\tau_P}e^{-\tau/\tau_P}\frac{1+e^{-(t_M-\tau)/\tau_P}}{1-e^{-(t_M-\tau)/\tau_P}} - 1. \tag{13}$$

In the third case (symmetric normalization), we obtain the following (36):

$$G_P(\tau) = \frac{t_M-\tau}{2\tau_P}\frac{1+e^{-(t_M-\tau)/\tau_P}}{1-e^{-(t_M-\tau)/\tau_P}} - 1. \tag{14}$$

AUTHOR CONTRIBUTIONS

L.Z. designed the research, performed and analyzed all the experiments, and wrote the manuscript. C.P.-R. designed the research and performed preliminary experiments. N.D. designed the research. C.F. designed the research, performed analytical calculations, and wrote the manuscript.

ACKNOWLEDGMENTS

L.Z. and C.P.-R. were both recipients of Ontario Trillium Scholarships. The research was funded by the Natural Sciences and Engineering Research Council of Canada through a discovery grant to C.F. (RGPIN-2015-06362).

REFERENCES

1. Berg, H. C., and E. M. Purcell. 1977. Physics of chemoreception. *Biophys. J.* 20:193–219.
2. Bialek, W., and S. Setayeshgar. 2005. Physical limits to biochemical signaling. *Proc. Natl. Acad. Sci. USA.* 102:10040–10045.
3. Houchmandzadeh, B., E. Wieschaus, and S. Leibler. 2002. Establishment of developmental precision and proportions in the early Drosophila embryo. *Nature.* 415:798–802.
4. Ashe, H. L., and J. Briscoe. 2006. The interpretation of morphogen gradients. *Development.* 133:385–394.
5. Gregor, T., E. F. Wieschaus, …, D. W. Tank. 2007. Stability and nuclear dynamics of the bicoid morphogen gradient. *Cell.* 130:141–152.
6. Kicheva, A., P. Pantazis, …, M. González-Gaitán. 2007. Kinetics of morphogen gradient formation. *Science.* 315:521–525.
7. Harvey, S. A., and J. C. Smith. 2009. Visualisation and quantification of morphogen gradient formation in the zebrafish. *PLoS Biol.* 7:e1000101.
8. Sagner, A., and J. Briscoe. 2017. Morphogen interpretation: concentration, time, competence, and signaling dynamics. *Wiley Interdiscip. Rev. Dev. Biol.* 6:e271.
9. Shilo, B.-Z., and N. Barkai. 2017. Buffering global variability of morphogen gradients. *Dev. Cell.* 40:429–438.
10. Durrieu, L., D. Kirrmaier, …, M. Knop. 2018. Bicoid gradient formation mechanism and dynamics revealed by protein lifetime analysis. *Mol. Syst. Biol.* 14:e8355.
11. Elson, E. L., and D. Magde. 1974. Fluorescence correlation spectroscopy. I. Conceptual basis and theory. *Biopolymers.* 13:1–27.
12. Maiti, S., U. Haupts, and W. W. Webb. 1997. Fluorescence correlation spectroscopy: diagnostics for sparse molecules. *Proc. Natl. Acad. Sci. USA.* 94:11753–11757.
13. Weissman, M., H. Schindler, and G. Feher. 1976. Determination of molecular weights by fluctuation spectroscopy: application to DNA. *Proc. Natl. Acad. Sci. USA.* 73:2776–2780.
14. Koppel, D. E. 1974. Statistical accuracy in fluorescence correlation spectroscopy. *Phys. Rev. A.* 10:1938–1945.
15. Rigler, R., Ü. Mets, …, P. Kask. 1993. Fluorescence correlation spectroscopy with high count rate and low background: analysis of translational diffusion. *Eur. Biophys. J.* 22:169–175.
16. Wachsmuth, M., T. Weidemann, …, J. Langowski. 2003. Analyzing intracellular binding and diffusion with continuous fluorescence photobleaching. *Biophys. J.* 84:3353–3363.
17. Delon, A., Y. Usson, …, C. Souchier. 2006. Continuous photobleaching in vesicles and living cells: a measure of diffusion and compartmentation. *Biophys. J.* 90:2548–2562.
18. Abu-Arish, A., A. Porcher, …, C. Fradin. 2010. High mobility of bicoid captured by fluorescence correlation spectroscopy: implication for the rapid establishment of its gradient. *Biophys. J.* 99:L33–L35.
19. Hodges, C., R. P. Kafle, …, J.-C. Meiners. 2018. Fluorescence correlation spectroscopy with photobleaching correction in slowly diffusing systems. *J. Fluoresc.* 28:505–511.
20. Sezgin, E., F. Schneider, …, C. Eggeling. 2019. Measuring nanoscale diffusion dynamics in cellular membranes with super-resolution STED-FCS. *Nat. Protoc.* 14:1054–1083.
21. Widengren, J., and R. Rigler. 1998. Fluorescence correlation spectroscopy as a tool to investigate chemical reactions in solutions and on cell surfaces. *Cell. Mol. Biol.* 44:857–879.
22. Delon, A., Y. Usson, …, C. Souchier. 2004. Photobleaching, mobility, and compartmentalisation: inferences in fluorescence correlation spectroscopy. *J. Fluoresc.* 14:255–267.
23. Wachsmuth, M., C. Conrad, …, J. Ellenberg. 2015. High-throughput fluorescence correlation spectroscopy enables analysis of proteome dynamics in living cells. *Nat. Biotechnol.* 33:384–389.
24. Waithe, D., F. Schneider, …, C. Eggeling. 2018. Optimized processing and analysis of conventional confocal microscopy generated scanning FCS data. *Methods.* 140–141:62–73.
25. Ries, J., S. Chiantia, and P. Schwille. 2009. Accurate determination of membrane dynamics with line-scan FCS. *Biophys. J.* 96:1999–2008.
26. Fradin, C., A. Abu-Arish, …, M. Elbaum. 2003. Fluorescence correlation spectroscopy close to a fluctuating membrane. *Biophys. J.* 84:2005–2020.
27. Cluzel, P., M. Surette, and S. Leibler. 2000. An ultrasensitive bacterial motor revealed by monitoring signaling proteins in single cells. *Science.* 287:1652–1655.
28. Weidemann, T., M. Wachsmuth, …, J. Langowski. 2003. Counting nucleosomes in living cells with a combination of fluorescence correlation spectroscopy and confocal imaging. *J. Mol. Biol.* 334:229–240.
29. Abu-Arish, A., P. Kalab, …, C. Fradin. 2009. Spatial distribution and mobility of the Ran GTPase in live interphase cells. *Biophys. J.* 97:2164–2178.
30. Politi, A. Z., Y. Cai, …, J. Ellenberg. 2018. Quantitative mapping of fluorescently tagged cellular proteins using FCS-calibrated four-dimensional imaging. *Nat. Protoc.* 13:1445–1464.
31. Heim, R., and R. Y. Tsien. 1996. Engineering green fluorescent protein for improved brightness, longer wavelengths and fluorescence resonance energy transfer. *Curr. Biol.* 6:178–182.
32. Kremers, G.-J., J. Goedhart, …, T. W. Gadella, Jr. 2007. Improved green and blue fluorescent proteins for expression in bacteria and mammalian cells. *Biochemistry.* 46:3775–3783.
33. Nagy, A., J. Wu, and K. M. Berland. 2005. Observation volumes and γ-factors in two-photon fluorescence fluctuation spectroscopy. *Biophys. J.* 89:2077–2090.
34. Widengren, J., U. Mets, and R. Rigler. 1995. Fluorescence correlation spectroscopy of triplet states in solution: a theoretical and experimental study. *J. Phys. Chem.* 99:13368–13379.
35. Wachsmuth, M., W. Waldeck, and J. Langowski. 2000. Anomalous diffusion of fluorescent probes inside living cell nuclei investigated by spatially-resolved fluorescence correlation spectroscopy. *J. Mol. Biol.* 298:677–689.
36. Bacia, K. 2005. Dynamic processes in membranes studied by fluorescence correlation spectroscopy. Technische Universität Dresden, PhD thesis.
37. Petrásek, Z., and P. Schwille. 2008. Precise measurement of diffusion coefficients using scanning fluorescence correlation spectroscopy. *Biophys. J.* 94:1437–1448.
38. Perez-Romero, C. A., H. Tran, …, N. Dostatni. 2018. Live imaging of mRNA transcription in Drosophila embryos. *In* Morphogen Gradients J. Dubrulle, ed.. Springer, pp. 165–182.
39. Patel, A. L., L. Zhang, …, S. Y. Shvartsman. 2021. A fast-acting transcriptional brake in the Drosophila embryo. *Curr. Biol.* Published online June 23, 2021. https://doi.org/10.1016/j.cub.2021.05.061.
40. Porcher, A., A. Abu-Arish, …, N. Dostatni. 2010. The time to measure positional information: maternal hunchback is required for the

synchrony of the Bicoid transcriptional response at the onset of zygotic transcription. *Development.* 137:2795–2804.

41. Vukojević, V., D. K. Papadopoulos, …, R. Rigler. 2010. Quantitative study of synthetic Hox transcription factor-DNA interactions in live cells. *Proc. Natl. Acad. Sci. USA.* 107:4093–4098.

42. Grimm, O., V. Sanchez Zini, …, E. Wieschaus. 2012. Torso RTK controls Capicua degradation by changing its subcellular localization. *Development.* 139:3962–3968.

43. Eggeling, C., J. Widengren, …, C. A. Seidel. 1998. Photobleaching of fluorescent dyes under conditions used for single-molecule detection: evidence of two-step photolysis. *Anal. Chem.* 70:2651–2659.

44. Dittrich, P., and P. Schwille. 2001. Photobleaching and stabilization of. fluorophores used for single-molecule analysis. with one-and two-photon excitation. *Appl. Phys. B.* 73:829–837.

45. Satsoura, D., B. Leber, …, C. Fradin. 2007. Circumvention of fluorophore photobleaching in fluorescence fluctuation experiments: a beam scanning approach. *Chemphyschem.* 8:834–848.

46. Hess, S. T., and W. W. Webb. 2002. Focal volume optics and experimental artifacts in confocal fluorescence correlation spectroscopy. *Biophys. J.* 83:2300–2317.

47. Nishimura, G., and M. Kinjo. 2004. Systematic error in fluorescence correlation measurements identified by a simple saturation model of fluorescence. *Anal. Chem.* 76:1963–1970.

48. Enderlein, J., I. Gregor, …, U. B. Kaupp. 2005. Performance of fluorescence correlation spectroscopy for measuring diffusion and concentration. *ChemPhysChem.* 6:2324–2336.

49. Nagy, A., J. Wu, and K. M. Berland. 2005. Characterizing observation volumes and the role of excitation saturation in one-photon fluorescence fluctuation spectroscopy. *J. Biomed. Opt.* 10:44015.

50. Berland, K. M., P. T. So, …, E. Gratton. 1996. Scanning two-photon fluctuation correlation spectroscopy: particle counting measurements for detection of molecular aggregation. *Biophys. J.* 71:410–420.

51. Friaa, O., M. Furukawa, …, C. Fradin. 2013. Optimizing the acquisition and analysis of confocal images for quantitative single-mobile-particle detection. *ChemPhysChem.* 14:2476–2490.